

See discussions, stats, and author profiles for this publication at: <https://www.researchgate.net/publication/285369818>

Controlled Formation of Metal@Al₂O₃ Yolk–Shell Nanostructures with Improved Thermal Stability

ARTICLE in ACS APPLIED MATERIALS & INTERFACES · NOVEMBER 2015

Impact Factor: 6.72 · DOI: 10.1021/acsaami.5b09791

READS

4

6 AUTHORS, INCLUDING:



Wei Zhang

Chinese Academy of Sciences

10 PUBLICATIONS 35 CITATIONS

[SEE PROFILE](#)

Controlled Formation of Metal@Al₂O₃ Yolk–Shell Nanostructures with Improved Thermal Stability

Wei Zhang,^{†,‡} Xi-Jie Lin,^{†,§} Yong-Gang Sun,^{†,‡} De-Shan Bin,^{†,‡} An-Min Cao,^{*,†} and Li-Jun Wan^{*,†}

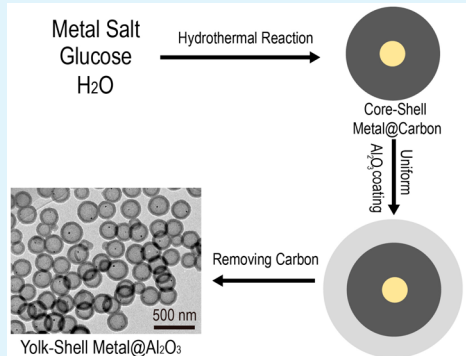
⁴ Key Laboratory of Molecular Nanostructure and Nanotechnology and Beijing National Laboratory for Molecular Sciences, Institute
5 of Chemistry, Chinese Academy of Sciences (CAS), Beijing 100190, P. R. China

⁶ University of Chinese Academy of Sciences, Beijing 100049, P. R. China

⁷ State Key Laboratory of Fine Chemicals, Dalian University of Technology, Dalian, China

Supporting Information

ABSTRACT: Yolk–shell structured nanomaterials have shown interesting potential in different areas due to their unique structural configurations. A successful construction of such a hybrid structure relies not only on the preparation of the core materials, but also on the capability to manipulate the outside wall. Typically, for Al₂O₃, it has been a tough issue in preparing it into a uniform nanoshell, making the use of Al₂O₃-based yolk–shell structures a challenging but long-awaited task. Here, in benefit of our success in the controlled formation of Al₂O₃ nanoshell, we demonstrated that yolk–shell structures with metal confined inside a hollow Al₂O₃ nanosphere could be successfully achieved. Different metals including Au, Pt, Pd have been demonstrated, forming a typical core@void@shell structure. We showed that the key parameters of the yolk–shell structure such as the shell thickness and the cavity size could be readily tuned. Due to the protection of a surrounding Al₂O₃ shell, the thermal stability of the interior metal nanoparticles could be substantially improved, resulting in promising performance for the catalytic CO oxidation as revealed by our preliminary test on Au@Al₂O₃.



KEYWORDS: *yolk–shell structure, Al₂O₃ coating, CO oxidation, catalysis, thermal stability*

Recently, yolk–shell or rattle-type have attracted significant attention for their potential applications in energy storage, catalysis, biomedical fields etc.^{1–7} These composite structures not only own superior properties that are beyond their individual-component counterparts, but also make it quite easy to tune various properties for different kinds of application functions.^{8–10} For example, these yolk–shell structures can effectively isolate each core, inhibit the deactivation caused by sintering of noble metals and maintain superior catalytic activity even at high-temperature heat treatment.¹¹ Meanwhile, using pH-sensitive materials for surface modification and tuning the hydrophilic ability of the shell enables us to readily and effectively achieve targeted drug delivery and controlled release of the core.¹²

In terms of oxides-based yolk–shell nanostructures, although some pioneering work has been done on constructing different oxides shell from SiO₂ to ZrO₂ and TiO₂, etc.,^{13–20} it is still very challenging to synthesize decent surface shells of other oxides, e.g., Al₂O₃. As is known to all, aluminum oxide is widely used as catalyst support, filler, and abrasive for many industrial applications because of its superior properties, such as superior stability, high specific surface area, low cost, etc.^{21,22} Constructing Al₂O₃-based yolk–shell structure not only could make up the blank of the family of these oxide composites but also might give some inspiration for potential practical

applications. The difficulty lies in lacking an effective method to develop a decent Al₂O₃ shell on the surface of seeds instead of forming separated nanoparticles, considering the high reactivity of aluminum alkoide and low solubility-product constants of aluminum hydroxide. How to effectively control the kinetic process of the deposition, well inhibit fast self-nucleation, and achieve gradual growth of Al₂O₃ is the key.

Herein, we demonstrate a facile synthetic protocol to construct noble metal-based yolk–shell structures with Al₂O₃ as the nanoshell (denoted by y-M@Al₂O₃). Such a control capability lies in our success in controlling the formation kinetics of Al(OH)₃ by using a suitable buffer solution as a unique growth media.²³ Following this preparation route, different metal nanoparticles such as Au, Pt, Pd, et al., could be successfully caged into a hollow Al₂O₃ nanospheres with tunable shell thickness and cavity size. We identified that the thermal stability of the encapsulated metal nanoparticles can be substantially improved in benefit of the protection of Al₂O₃. The preliminary test on the catalytic performance of y-Au@Al₂O₃ showed such a yolk–shell structured nanocomposite

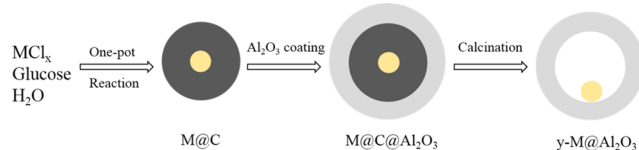
Received: October 14, 2015

Accepted: November 30, 2015

71 could be a promising candidate for a stable catalyst toward CO
72 oxidation.

73 A brief illustration for our synthesis route could be found in
74 Scheme 1. First, a one-pot hydrothermal reaction was adopted

Scheme 1. Schematic Illustration of the Preparation of y-M@Al₂O₃ Yolk–Shell Nanostructure



75 to prepare a core–shell structure of M@C (metal core, carbon
76 shell),²⁴ which was then used as seeds for the following surface
77 growth of Al₂O₃. By dispersing these M@C nanoparticles in a
78 buffer solution of formic acid-ammonium formate, uniform
79 Al(OH)₃ layers could gradually grow onto their surface by
80 controlling its precipitation process and then a core–shell
81 structure with two coating layers of both carbon and Al₂O₃
82 formed. Finally, the intermediate carbon layers were burnt off
83 to achieve the target product y-M@Al₂O₃. The existence of
84 carbon on the M surface played at least a double role in our
85 synthesis. On one hand, it can make the M@C seeds highly
86 hydrophilic because of their abundant hydroxyl groups. In this
87 way, the sample could be easily dispersed in the solution to
88 achieve a possible Al₂O₃ coating. On the other hand, the cavity
89 size of the final product of y-M@Al₂O₃ could be easily
90 controlled by changing the thickness of the preformed carbon
91 coating.

92 As revealed by the typical transmission electron microscopy
93 (TEM) image of Au@C (Figure 1a), the synthesized

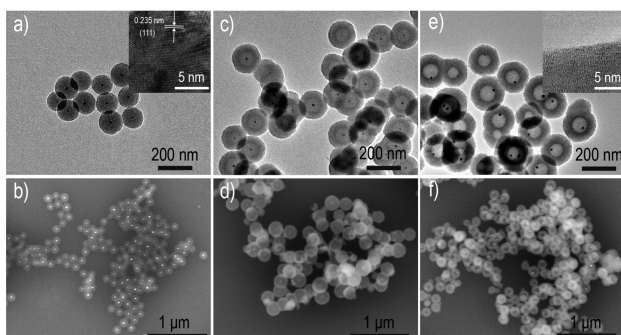


Figure 1. (a, c, e) TEM and (b, d, f) SEM-BSE images of the products achieved at different stages: (a, b) Au@C, (c, d) Au@C@Al₂O₃, (e, f) y-Au@Al₂O₃. The inset of a and e are HRTEM images of Au core and Al₂O₃ shell, respectively.

94 nanoparticles are relatively uniform with the average diameter
95 of ~120 nm and the majority of carbon spheres contain only
96 one ~15 nm gold nanoparticle in the center, respectively.
97 Figure 1b shows the corresponding scanning electron
98 microscopy (SEM) image of Au@C obtained with back-
99 scattered electrons (BSE). The inner bright spots represent the
100 gold cores and the dark spheres correspond to the carbon
101 shells, because of the significant difference in the atomic
102 number between element Au and C. The diameter of the dark
103 spheres is about 120 nm and there obviously exists one bright
104 spot in the center of almost every dark sphere, which are
105 consistent with the above TEM results. After Al₂O₃ surface

coating process, about 40 nm thick amorphous layer grows 106 continuously and uniformly around Au@C nanospheres 107 (Figure 1c). Because there are double coating layers on the 108 surface of Au nanoparticles, the contrast between gold core and 109 outer shell is no longer obvious but still can be distinguished in 110 the SEM-BSE image (Figure 1d). Figure 1e, f demonstrates the 111 TEM and SEM-BSE images of the final product y-Au@Al₂O₃. 112 Considering that the carbon scaffold that immobilized the gold 113 nanoparticles does not exist any longer after heat treatment, the 114 core particles naturally deposit from the center of the hollow 115 alumina spheres. The size of the void is slightly less than that of 116 original carbon probably because of the little shrinkage during 117 high-temperature annealing.
118

Figure 2a shows the X-ray diffraction (XRD) pattern of the 119 synthesized y-Au@Al₂O₃ nanoparticles. The weak but dis- 120

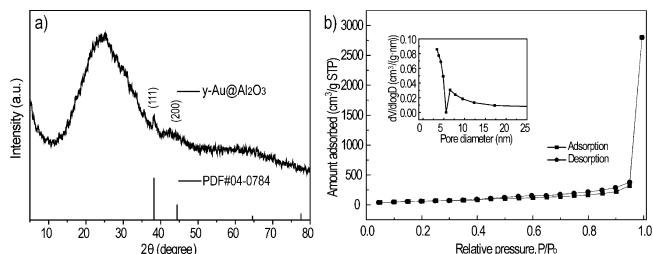


Figure 2. (a) XRD patterns and (b) N₂ sorption isotherms as well as the pore size distribution (inset) of the prepared y-Au@Al₂O₃ yolk–shell nanostructure.

cernible peaks accord well with small-size gold nanoparticles 121 (PDF#04-0784). The broad peak at around 26 degree and no 122 other additional one verify the amorphous property of alumina 123 shells, which is in good agreement with the previous result.²³ 124 The N₂ adsorption–desorption isotherms of y-Au@Al₂O₃ 125 nanostructures (Figure 2b) exhibit representative type IV 126 curves with a hysteresis loop in relative pressure range of 0.3– 127 0.95, implying a broad pore size distribution. The Brunauer– 128 Emmett–Teller (BET) surface area and the pore volume of y- 129 Au@Al₂O₃ are about 228 m²/g and 4.367 cm³/g, respectively. 130 What's more, the average diameter of the mesopore is 131 calculated to be 3.4 nm from the desorption branch based on 132 the Barrett–Joyner–Halenda (BJH) method (Figure 2b, inset). 133

To further demonstrate this Al₂O₃-based yolk–shell 134 nanostructure, elemental mappings were carried out on three 135 randomly picked spheres in the scanning TEM (STEM) mode. 136 As revealed in Figure 3a–d, Al as well as O distributes 137 f3

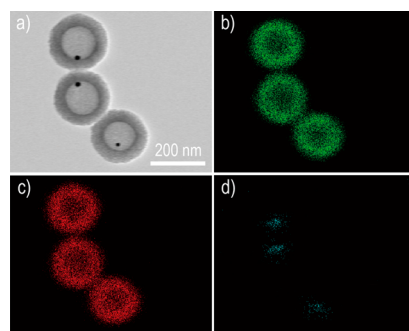


Figure 3. STEM characterization of three representative y-Au@Al₂O₃ nanospheres: (a) morphology mode of STEM image, (b–d) elemental mappings of (b) Al, (c) O, and (d) Au on these three particles.

homogeneously on the shell and Au can also be clearly identified somewhere inside each sphere, confirming the presence of alumina shell and gold core. The brighter edge further demonstrates the hollow characteristics of the aluminum oxide spheres.

Additionally, the cavity size and shell thickness of $\text{y-Au}@\text{Al}_2\text{O}_3$ were determined by the diameter of carbon spheres and amount of alumina deposition, which could be easily and precisely tuned by varying the synthetic conditions such as the reaction time and the concentration. As shown by the TEM images in Figure 4a, b, the diameter of carbon increase to 200

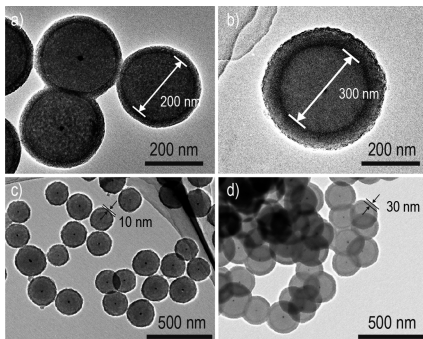


Figure 4. TEM images of $\text{Au}@\text{C}@\text{Al}_2\text{O}_3$ with (a, b) different carbon sphere diameter and (c, d) various alumina shell thickness.

and 300 nm when prolonging the process of the hydrothermal reaction. Meanwhile, changing the concentration of aluminum salts or the reaction time, the thickness of Al_2O_3 nanoshell also could be well controlled (Figure 4c, d) and the coating layers are still uniform, continuous, and smooth.

In addition, this synthetic route of $\text{y-Au}@\text{Al}_2\text{O}_3$ can also be applicable for other metal core. When the metal precursor HAuCl_4 is replaced by other corresponding inorganic salts such as H_2PtCl_6 and $(\text{NH}_4)_2\text{PdCl}_4$ and other synthetic conditions almost remain unchanged, the corresponding $\text{y-Pt}@\text{Al}_2\text{O}_3$ and $\text{y-Pd}@\text{Al}_2\text{O}_3$ yolk–shell structures could be readily achieved (Figure 5a, b).

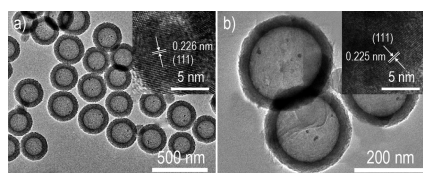


Figure 5. TEM images of $\text{y-M}@\text{Al}_2\text{O}_3$ yolk–shell nanostructure with various metal core: (a) Pt, (b) Pd.

The CO oxidation, one of the standard reactions for gold catalyst, was investigated on this prepared $\text{y-Au}@\text{Al}_2\text{O}_3$ nanocatalyst. Figure 6a shows the plots of CO conversion ratio versus reaction temperature over $\text{y-Au}@\text{Al}_2\text{O}_3$ annealed at 550 °C, 800 °C and $\text{Au}/\text{Al}_2\text{O}_3$ annealed at 800 °C prepared by the impregnation method as well as blank Al_2O_3 sample. All these samples show low catalytic activity below 150 °C probably due to the large size of Au. Generally speaking, only when the particles size is smaller than 5 nm can gold nanoparticles show high catalytic activity. Considering the large size (~15 nm) and the low loading (~0.5 wt %) of metal cores, the catalytic performance of CO oxidation over our prepared $\text{y-Au}@\text{Al}_2\text{O}_3$ nanocatalyst is acceptable and satisfying,

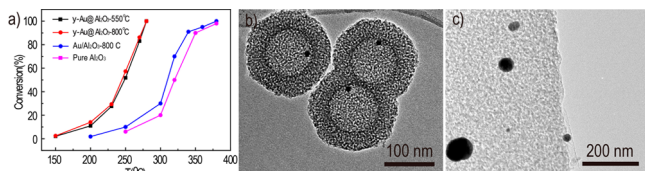


Figure 6. (a) Catalytic activity of $\text{y-Au}@\text{Al}_2\text{O}_3$ nanocatalyst annealed at 550 °C, 800 °C, $\text{Au}/\text{Al}_2\text{O}_3$ annealed at 800 °C and blank Al_2O_3 for CO oxidation. Feed gas containing 1 vol % CO, 21 vol % O_2 , and balance He is at a flow rate of $50 \text{ cm}^3 \text{ min}^{-1}$, corresponding to a space velocity of $60\,000 \text{ cm}^3 \text{ h}^{-1} \text{ g}_{\text{cat}}^{-1}$. (b, c) TEM image of (b) $\text{y-Au}@\text{Al}_2\text{O}_3$ yolk–shell nanostructures and (c) contrast sample $\text{Au}/\text{Al}_2\text{O}_3$ after heat treatment at 800 °C for 2 h.

which may be ascribed to the inner void and outer mesoporous shells of this yolk–shell nanostructure. In addition, the catalytic activity of this nanocatalyst is well-maintained even after annealing at 800 °C, whereas that of $\text{Au}/\text{Al}_2\text{O}_3$ decreases obviously because of the seriously sintering of metal. As demonstrated by the corresponding TEM images of both samples after high-temperature treatment (Figure 6b, c), the yolk–shell nanostructure of $\text{y-Au}@\text{Al}_2\text{O}_3$ does not crush and the size of gold core is essentially unchanged, whereas the Au particles size of the contrast sample obviously and substantially increased, demonstrating that the stable alumina shells of yolk–shell structure well-isolate each core and effectively inhibit sintering and aggregation of gold nanoparticles.

In summary, we have developed a facile synthetic protocol to construct $\text{y-M}@\text{Al}_2\text{O}_3$ yolk–shell nanostructure. M@C core–shell nanospheres were first prepared via a one-pot hydrothermal method and then uniform aluminum oxide layers were gradually deposited around the surface of these nanospheres by using buffer solution as a specific reaction media. Finally, the target product $\text{y-M}@\text{Al}_2\text{O}_3$ were achieved by selectively burning off the carbon layer. The cavity size and shell thickness of this yolk–shell nanostructure can be readily and precisely tuned by varying the corresponding synthetic conditions. The prepared $\text{y-Au}@\text{Al}_2\text{O}_3$ nanocatalyst shows an acceptable and satisfied catalytic activity on CO oxidation, taking the large size and the low loading of gold into account. Additionally, the alumina shells well-isolated each gold nanoparticle and effectively inhibit the aggregation and sintering of Au cores even after high-temperature treatment.

ASSOCIATED CONTENT

Supporting Information

The Supporting Information is available free of charge on the ACS Publications website at DOI: 10.1021/acsami.5b09791.

Complementary TEM images of $\text{Pd}@\text{C}$, XRD of pure alumina and EDS of $\text{y-M}@\text{Al}_2\text{O}_3$ yolk–shell structures (PDF)

AUTHOR INFORMATION

Corresponding Authors

*E-mail: anmin_cao@iccas.ac.cn.

*E-mail: wanlijun@iccas.ac.cn.

Notes

The authors declare no competing financial interest.

ACKNOWLEDGMENTS

This work was supported by the major State Basic Research Program of China (973 program: 2013CB934000, 863

219 program: 2013AA030800), the National Natural Science
220 Foundation of China (Grant 21373238), and the Chinese
221 Academy of Sciences (XDA09010001).

222 ■ REFERENCES

- 223 (1) Caruso, F.; Caruso, R. A.; Möhwald, H. Nanoengineering of
224 Inorganic and Hybrid Hollow Spheres by Colloidal Templating.
225 *Science* **1998**, *282* (5391), 1111–1114.
- 226 (2) Ghosh Chaudhuri, R.; Paria, S. Core/Shell Nanoparticles:
227 Classes, Properties, Synthesis Mechanisms, Characterization, and
228 Applications. *Chem. Rev.* **2012**, *112* (4), 2373–2433.
- 229 (3) Liu, N.; Lu, Z.; Zhao, J.; McDowell, M. T.; Lee, H. W.; Zhao, W.;
230 Cui, Y. A Pomegranate-Inspired Nanoscale Design for Large-Volume-
231 Change Lithium Battery Anodes. *Nat. Nanotechnol.* **2014**, *9* (3), 187–
232 192.
- 233 (4) Kalele, S.; Gosavi, S.; Urban, J.; Kulkarni, S. Nanoshell Particles:
234 Synthesis, Properties and Applications. *Curr. Sci.* **2006**, *91* (8), 1038–
235 1052.
- 236 (5) Priebe, M.; Fromm, K. M. Nanorattles or Yolk–Shell
237 Nanoparticles—What Are They, How Are They Made, and What
238 Are They Good For? *Chem. - Eur. J.* **2015**, *21* (10), 3854–3874.
- 239 (6) Sindoro, M.; Granick, S. Voids and Yolk-Shells from Crystals
240 That Coat Particles. *J. Am. Chem. Soc.* **2014**, *136* (39), 13471–13473.
- 241 (7) Lee, J.; Kim, S. M.; Lee, I. S. Functionalization of Hollow
242 Nanoparticles for Nanoreactor Applications. *Nano Today* **2014**, *9* (5),
243 631–667.
- 244 (8) He, L.; Liu, Y.; Liu, J.; Xiong, Y.; Zheng, J.; Liu, Y.; Tang, Z.
245 Core–Shell Noble-Metal@Metal–Organic-Framework Nanoparticles
246 with Highly Selective Sensing Property. *Angew. Chem., Int. Ed.* **2013**,
247 *52* (13), 3741–3745.
- 248 (9) Zhao, M.; Deng, K.; He, L.; Liu, Y.; Li, G.; Zhao, H.; Tang, Z.
249 Core–Shell Palladium Nanoparticle@Metal–Organic Frameworks as
250 Multifunctional Catalysts for Cascade Reactions. *J. Am. Chem. Soc.*
251 **2014**, *136* (5), 1738–1741.
- 252 (10) Sun, Z.; Xie, K.; Li, Z. A.; Sinev, I.; Ebbinghaus, P.; Erbe, A.;
253 Farle, M.; Schuhmann, W.; Muhler, M.; Ventosa, E. Hollow and Yolk–
254 Shell Iron Oxide Nanostructures on Few-Layer Graphene in Li-Ion
255 Batteries. *Chem. - Eur. J.* **2014**, *20* (7), 2022–2030.
- 256 (11) Arnal, P. M.; Comotti, M.; Schüth, F. High-Temperature-Stable
257 Catalysts by Hollow Sphere Encapsulation. *Angew. Chem., Int. Ed.*
258 **2006**, *45* (48), 8224–8227.
- 259 (12) Fang, Y.; Zheng, G.; Yang, J.; Tang, H.; Zhang, Y.; Kong, B.; Lv,
260 Y.; Xu, C.; Asiri, A. M.; Zi, J.; Zhang, F.; Zhao, D. Dual-Pore
261 Mesoporous Carbon@Silica Composite Core–Shell Nanospheres for
262 Multidrug Delivery. *Angew. Chem.* **2014**, *126* (21), 5470–5474.
- 263 (13) Kamata, K.; Lu, Y.; Xia, Y. Synthesis and Characterization of
264 Monodispersed Core–Shell Spherical Colloids with Movable Cores. *J.*
265 *Am. Chem. Soc.* **2003**, *125* (9), 2384–2385.
- 266 (14) Yu, M.; Liang, C.; Liu, M.; Liu, X.; Yuan, K.; Cao, H.; Che, R.
267 Yolk–Shell $\text{Fe}_3\text{O}_4@\text{ZrO}_2$ prepared by a Tunable Polymer Surfactant
268 Assisted Sol–Gel Method for High Temperature Stable Microwave
269 Absorption. *J. Mater. Chem. C* **2014**, *2* (35), 7275.
- 270 (15) Wang, S.; Zhang, M.; Zhang, W. Yolk–Shell Catalyst of Single
271 Au Nanoparticle Encapsulated within Hollow Mesoporous Silica
272 Microspheres. *ACS Catal.* **2011**, *1* (3), 207–211.
- 273 (16) Yu, K.; Wu, Z.; Zhao, Q.; Li, B.; Xie, Y. High-Temperature-
274 Stable $\text{Au}@\text{SnO}_2$ Core/Shell Supported Catalyst for CO Oxidation. *J.*
275 *Phys. Chem. C* **2008**, *112* (7), 2244–2247.
- 276 (17) Shevchenko, E. V.; Bodnarchuk, M. I.; Kovalenko, M. V.;
277 Talapin, D. V.; Smith, R. K.; Aloni, S.; Heiss, W.; Alivisatos, A. P.
278 Gold/Iron Oxide Core/Hollow-Shell Nanoparticles. *Adv. Mater.* **2008**,
279 *20* (22), 4323–4329.
- 280 (18) Dillon, R. J.; Joo, J. B.; Zaera, F.; Yin, Y.; Bardeen, C. J.
281 Correlating the Excited State Relaxation Dynamics as Measured by
282 Photoluminescence and Transient Absorption with the Photocatalytic
283 Activity of $\text{Au}@\text{TiO}_2$ Core–Shell Nanostructures. *Phys. Chem. Chem.*
284 *Phys.* **2013**, *15* (5), 1488–1496.
- 285 (19) Chen, C.; Fang, X.; Wu, B.; Huang, L.; Zheng, N. A Multi-Yolk-
286 Shell Structured Nanocatalyst Containing Sub-10 nm Pd Nano-
287 particles in Porous CeO_2 . *ChemCatChem* **2012**, *4* (10), 1578–1586.
288 (20) Du, J.; Qi, J.; Wang, D.; Tang, Z. Facile Synthesis of $\text{Au}@\text{TiO}_2$
289 Core–Shell Hollow Spheres for Dye-Sensitized Solar Cells with
290 Remarkably Improved Efficiency. *Energy Environ. Sci.* **2012**, *5* (5),
291 6914–6918.
- 292 (21) Trueba, M.; Trasatti, S. P. γ -Alumina as a Support for Catalysts:
293 A Review of Fundamental Aspects. *Eur. J. Inorg. Chem.* **2005**, *2005*
294 (17), 3393–3403.
- 295 (22) Dingemans, G.; Kessels, W. M. M. Status and Prospects of
296 Al_2O_3 -Based Surface Passivation Schemes for Silicon Solar Cells. *J.*
297 *Vac. Sci. Technol., A* **2012**, *30* (4), 040802.
- 298 (23) Zhang, W.; Chi, Z. X.; Mao, W. X.; Lv, R. W.; Cao, A. M.; Wan,
299 L. J. One-Nanometer-Precision Control of Al_2O_3 Nanoshells through a
300 Solution-Based Synthesis Route. *Angew. Chem., Int. Ed.* **2014**, *53* (47),
301 12776–12780.
- 302 (24) Sun, X.; Li, Y. Colloidal Carbon Spheres and Their Core/Shell
303 Structures with Noble-Metal Nanoparticles. *Angew. Chem., Int. Ed.*
304 **2004**, *43* (5), 597–601.